Nano Research
2021, 14(12): 4841–4847
ISSN 1998-0124 CN 11-5974/O4
https://doi.org/10.1007/s12274-021-3443-7

Research Article

Dispersion and support dictated properties and activities of Pt/metal oxide catalysts in heterogeneous CO oxidation

Jiaojiao Song[1,§], Yixuan Yang[1,§], Shoujie Liu[2,3], Lei Li[4], Nan Yu[2], Yuteng Fan[1], Zhiming Chen[1], Long Kuai[1] (✉), and Baoyou Geng[2] (✉)

[1] School of Chemical and Environmental Engineering, Anhui Laboratory of Functional Coordinated Complexes for Materials Chemistry and Application, Anhui Laboratory of Clean Catalytic Engineering, Anhui Laboratory of Clean Energy Materials and Chemistry for Sustainable Conversion of Natural Resources, Anhui Polytechnic University, Wuhu 241000, China
[2] College of Chemistry and Materials Science, The key Laboratory of Functional Molecular Solids, Ministry of Education, the Key Laboratory of Electrochemical Clean Energy of Anhui Higher Education Institutes, Anhui Provincial Engineering Laboratory for New-Energy Vehicle Battery Energy-Storage Materials, Anhui Normal University, Wuhu 241002, China
[3] Chemistry and Chemical Engineering of Guangdong Laboratory, Shantou 515063, China
[4] Chongqing Key Laboratory of Extraordinary Coordination Bond and Advanced Materials Techniques, Yangtze Normal University, Chongqing 408100, China
[§] Jiaojiao Song and Yixuan Yang contributed equally to this work.

Received: 20 January 2021 / **Revised:** 2 March 2021 / **Accepted:** 7 March 2021

ABSTRACT

The source of activity of metal/metal oxides has always been an interesting, important but highly challenging research topic in heterogeneous catalysis. In CO oxidation reaction, this work clarifies dispersion and support dictated activities of Pt including single-atom (Pt_1), 2.8 nm ($Pt_{NP\text{-}S}$) and 36 nm ($Pt_{NP\text{-}L}$) Pt supported on both reducible TiO_2 and "inert" Al_2O_3 supports. The X-ray absorption fine structure (XAFS) shows that chemical state of Pt is affected by both dispersion and support: Pt_1 presents fully oxidized state in both Pt_1/TiO_2 and Pt_1/Al_2O_3; $Pt_{NP\text{-}S}$ in $Pt_{NP\text{-}S}/TiO_2$ appear nearly oxidized state while about half of Pt is metallic state in $Pt_{NP\text{-}S}/Al_2O_3$; $Pt_{NP\text{-}L}$ in both $Pt_{NP\text{-}L}/TiO_2$ and $Pt_{NP\text{-}L}/Al_2O_3$ exhibit metallic state. All the Pt species supported on TiO_2 present much lower apparent activation barriers (E_{app}) than that on Al_2O_3. Moreover, Pt_1/TiO_2 possesses dozen times of efficiency than $Pt_{NP\text{-}S}/TiO_2$ although they have similar E_{app} values. A truth is finally made clear that a reducible metal oxide with low oxygen vacancy formation energy is critical to endow Pt/metal oxide a high activity and the single-atom dispersion of Pt is the way to maximize the active sites of Pt/metal oxide.

KEYWORDS

nano catalysis, single-atom catalysis, platinum, dispersion, CO oxidation

1 Introduction

Supported Pt-based catalysts are critical to many industrial chemical processes like low-temperature (preferential) CO oxidation [1–4], hydrogenation [5–7], water-gas shift reaction [8, 9], steam reformation [10, 11] and so forth. To cope with the high cost and scarcity of noble metals including Pt, in the past decade, great efforts have been made to downsize active metals to atomically dispersed species for maximizing the metal efficiency [12–16]. Moreover, some single-atom sites have been identified as the active center in the reactions of water–gas shift reaction [17, 18], methanol/water reforming [11], oxygen and proton electroreduction [19–21], etc. Nevertheless, the debate is still raised on the activity of single-atom catalysts [22, 23]. Taking single atom Pt (Pt_1) catalysts toward low-temperature CO oxidation as example, some studies indicate that the active sites are Pt_1 sites instead of Pt nanoparticles (Pt_{NPs}) [4, 24] and many Pt_1 catalysts such as Pt_1/FeO_x and Pt_1/CeO_2 have been reported to working efficiently at a temperature lower than 80 °C [4, 5, 25, 26]. Sykes's group clearly demonstrated that it was the individual Pt atoms on Cu_2O film that response to the CO oxidation at low-temperature [24]. In contrast, several other works present that the Pt_1 catalysts work inefficiently for low-temperature CO oxidation. In Pt_1/Al_2O_3, a typically poor Pt_1 catalyst, the CO oxidation activity was not observed until the temperature rises higher than 200 °C [27, 28]. In particular, Stair et al. assigned the active sites in CO oxidation as Pt nanoparticles or clusters, while the spectators of single-atom Pt sites underwent the less efficient O_2 activation and strong CO adsorption [22, 29, 30]. To understand the above-discussed opposite results, we need a clear and definite nature of activity origins of Pt/metal oxides with size of Pt ranging from single-atom to dozens of nanometers.

Actually, the property of support is a well-known important factor to affect the property and activity of supported metal particles [31–33]. The metal/metal oxide interaction affects the chemical property of active metals and the surface lattice oxygen of reducible metal oxides even participates the pathway of some catalytic oxidation reactions through Mars-van Krevelen mechanism [34, 35]. In the previous work, the supports used

Address correspondence to Long Kuai, kuailong@ahpu.edu.cn; Baoyou Geng, bygeng@ahnu.edu.cn

for anchoring Pt_1 and exploring its activity are quite different. Interestingly, the negative results for Pt_1 catalysts always appear with "inert" metal oxide supports (e.g., Al_2O_3 and SiO_2), while the positive results are found with the reducible supports (e.g., Cu_2O and FeO_x). Nevertheless, the knowledge of influence of dispersity of active metals is of equal importance [36, 37]. The dispersity greatly affects the chemical state and surface property of supported active metals, which determines the catalytic behaviors [38, 39]. To the best of our knowledge, all the observed single atom metals supported on metal oxides present completely oxidized state, while the supported large nanocrystals remain metallic property [4, 27, 40]. Therefore, a knowledge on the role of dual dispersion and support is critical to further understand the activity origin of Pt/metal oxide and response the debate on Pt_1/metal oxide catalysts. Because the structure and property of catalysts are highly sensitive to the preparation method and metal loading, it is of great difficulty to study the dual dispersion and support regulated property and activity of Pt/metal oxide catalysts. It is unlikely to obtain pure Pt nanoparticles/metal oxide catalysts without any Pt_1 or clusters by conventional immersion/deposition or co-precipitation methods [41–43]. In order to eliminate the effect of methodology as low as possible and get a reliable experimental result and fundamental knowledge, the primary issue is preparing Pt/metal oxide catalysts by a uniform method and controlling monodispersity of Pt species ranging from single-atom to dozens of nanometers.

Herein, an efficient synchronous spray-pyrolysis deposition route (SPDR, Scheme 1) was put forward to prepare Pt/metal oxides catalysts. Reported in our previous work [40, 44–46], SPDR is available to fabricate various mesoporous oxides supported single atoms or transfer metal particles from colloid solution onto metal oxide support. Especially, the SPDR eliminates the barrier for preparing pure Pt nanoparticles/metal oxide catalysts by using colloid solution as precursor. Herein, TiO_2 and Al_2O_3 are selected to represent the reducible and inert supports, respectively. The Pt_1/TiO_2 and Pt_1/Al_2O_3 single-atom catalysts were prepared with a precursor of H_2PtCl_6. The nanosized Pt/TiO_2 and Pt/Al_2O_3 catalysts were obtained with the Pt colloids [47, 48] as precursor. Both small Pt particles ($Pt_{NP\text{-}S}$) and large Pt ($Pt_{NP\text{-}L}$) nanocrystals can be transferred and embedded into TiO_2 and Al_2O_3 matrix, marked as $Pt_{NP\text{-}S}/TiO_2$, $Pt_{NP\text{-}S}/Al_2O_3$, $Pt_{NP\text{-}L}/TiO_2$, and $Pt_{NP\text{-}L}/Al_2O_3$. SPDR ensures the consistency of material synthesis to prepare all the catalysts by SPDR for investing their properties. Furthermore, through X-ray absorption study and a model reaction of CO oxidation, the dual dispersion state and property of support is found to regulate the property and activity of Pt/metal oxide catalysts: a reducible metal oxide is critical to endow Pt–O–M site a high activity and the single-atom dispersion of Pt is the way to maximize Pt–O–M sites.

2 Experimental

Preparation of Pt_1/TiO_2: 0.93 mL of tetrabutyl titanate (TBT, Aladdin), 1 mL of concentrated hydrochloric acid (35%–37%), 0.5 g F127 ($PEO_{106}PPO_{70}PEO_{106}$, Sigma), and 1.0 mL of 10 mM H_2PtCl_6 were mixed in 40 mL deionized water by ultrasonic assistance. The obtained precursor solution was sprayed by a household ultrasonic atomizer (1.7 MHz, 35 W). The mist was brought into a reaction tube (600 °C, 30 cm) embedded in a furnace by a vacuum pump. At the end of reaction tube, a filter was used to collect the powder. The collected powder was further calcined in air at 400 °C for 2 hours (2 °C/min). The product was washed 3 times with H_2O and C_2H_5OH, respectively.

Preparation of Pt_1/Al_2O_3: The preparation procedure is same to Pt_1/TiO_2. The precursor solution was a mixture of 1.50 g $Al(NO_3)_3{\cdot}9H_2O$ (AR, Aladdin), 0.32 g F127, and 0.6 mL of 10 mM H_2PtCl_6 in 40 mL deionized water.

Preparation of $Pt_{NP\text{-}S}/TiO_2$: The preparation procedure is same to Pt_1/TiO_2. The precursor solution was a mixture of 0.93 mL of TBT, 1 mL of concentrated hydrochloric acid, 0.5 g F127, and 5.0 mL of concentrated $Pt_{NP\text{-}S}$ colloid in 40 mL deionized water.

Preparation of $Pt_{NP\text{-}L}/TiO_2$: The preparation procedure is same to Pt_1/TiO_2. The precursor solution was a mixture of 0.93 mL of TBT, 1 mL of concentrated hydrochloric acid, 0.5 g F127, and the prepared $Pt_{NP\text{-}L}$ colloid in 40 mL deionized water.

Preparation of $Pt_{NP\text{-}S}/Al_2O_3$: The preparation procedure is same to Pt_1/TiO_2. The precursor solution was a mixture of 1.50 g $Al(NO_3)_3{\cdot}9H_2O$, 0.32 g F127, and 5.0 mL of concentrated $Pt_{NP\text{-}S}$ colloid in 40 mL deionized water.

Preparation of $Pt_{NP\text{-}L}/Al_2O_3$: The preparation procedure is same to Pt_1/TiO_2. The precursor solution was a mixture of 1.50 g $Al(NO_3)_3{\cdot}9H_2O$, 0.32 g F127, and the prepared $Pt_{NP\text{-}L}$ colloid in 40 mL deionized water.

Catalytic CO oxidation tests: The tests were performed in a fixed-bed tube reactor at atmospheric pressure. Typically, 0.10 g of catalyst powder was diluted with 3 mL of quartz sands and filled into a quartz reaction tube (with 8 mm inner diameter and 30 cm length). The feed gas was a mixture of 1.0% CO, 1.0% O_2, and 98% balanced He. The feed flow was 25 mL/min controlled by a mass flowmeter. Prior to collecting the data, the catalysts were pre-treated at 300 °C *in-situ* to remove the organic adsorbates. After cooling down to the reaction temperature, the consuming of CO was measured by a He (99.99%) carried on-line gas chromatography (GC9790, Fuli

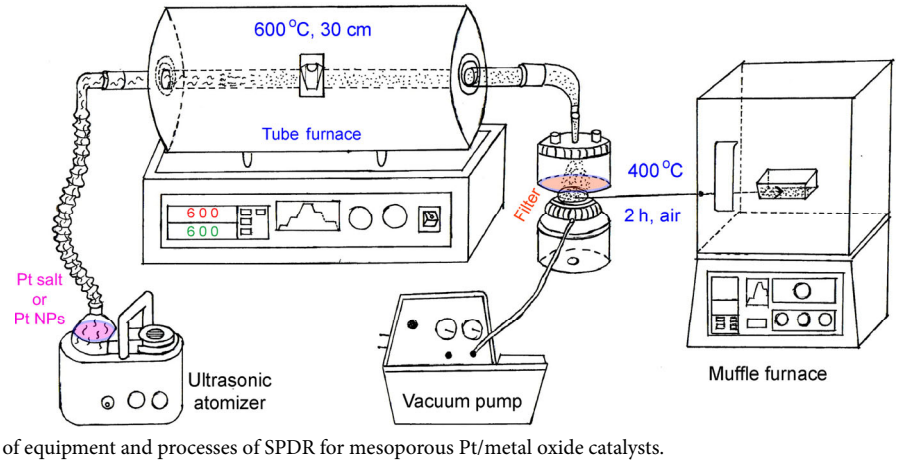

Scheme 1 Illustration of equipment and processes of SPDR for mesoporous Pt/metal oxide catalysts.

Instruments, China) equipped with a TDX-01 column (2.0 m in length and 4 mm in diameter) with working temperature of 110 °C and a TCD detector with working temperature/current of 120 °C/60 mA.

Method and model for DFT calculation: The first principles calculations of density functional theory were performed with Cambridge Sequential Total Energy Package (CASTEP) [49]. The generalized gradient approximation (GGA) [50] was considered as the exchange–correlation functional with norm-conserving pseudopotentials and Perdew–Burke–Ernzerhof (PBE) functional was adopted to describe the interaction between electrons [51]. The PBE functional is generally to deal with the electron state, and has been successfully used to study TiO_2 [52] and Al_2O_3 [53] surface, respectively. The energy cutoff was set to 450 eV and the k-point sampling was set to $5 \times 5 \times 1$. The requirement for convergence for geometry optimization to the ground state appears with a force tolerance of 0.01 eV/Å, an energy tolerance of 5.0×10^{-7} eV/atom, and a maximum displacement of 5.0×10^{-4} Å. In addition, the bottom three atomic layers are fixed and the top three atomic layers and adsorbates are relaxed. The vacuum space was set to be 15 Å along the *z* direction to avoid the interaction of images. For searching the transition states, the complete linear synchronous transit/quadratic synchronous transit (LST/QST) search protocol was performed, with a self-consistent field (SCF) tolerance of 1.0×10^{-6} eV per atom and root mean square (RMS) convergence of 0.05 eV/Å.

3 Results and discussion

The Pt/TiO_2 and Pt/Al_2O_3 catalysts were prepared for a case study of Pt supported on reducible and "inert" metal oxides, respectively. As illustrated in Scheme 1, assisted by an ultrasonic atomizer, the precursor solution containing Ti (or Al) source, H_2PtCl_6 (or pre-prepared Pt nanoparticles), and Pluronic F127 was sprayed and driven into a tube furnace with heating zone of 30 cm at 600 °C. The mist containing precursor microdrops was dried and the Ti (or Al) source in the precursor was pyrolyzed to generate TiO_2 (or Al_2O_3) *in situ*. Meanwhile, the Pt atoms or pre-prepared Pt nanoparticles were deposited on the supports. The powder was collected with a filter driven by a vacuum pump and subsequently calcined in air to remove the F127 template and obtain mesoporous catalysts. Figures 1(a) and (b) show the high-magnification aberration-corrected high-angle annular dark field scanning transmission electron microscope (AC-HAADF-STEM) images of SPDR-made Pt_1/TiO_2 and Pt_1/Al_2O_3 catalysts. The single Pt atoms (brighter spots) are anchored on the walls of TiO_2 or Al_2O_3 matrix with mesoporous microspheres structure (Figs. S1 and S2 in the Electronic Supplementary Material (ESM)). Figure 1(c) displays the HAADF-STEM image of pre-prepared $Pt_{NP\text{-}S}$ with size distribution centered at 2.8 ± 0.5 nm (Fig. 1(d)). In both HAADF-STEM (Fig. 1(e)) and TEM images (Fig. S3 in the ESM) of SPDR-made $Pt_{NP\text{-}S}/Al_2O_3$ catalyst, $Pt_{NP\text{-}S}$ are clearly observed in a microsphere and the size is consistent with the prepared $Pt_{NP\text{-}S}$. In SPDR- made $Pt_{NP\text{-}S}/TiO_2$ catalyst, $Pt_{NP\text{-}S}$ are also distinguished clearly from TiO_2 matrix in AC-HAADF-STEM (Fig. 1(f)) and AC-TEM (Fig. S4 in the ESM) images. The 0.26 wt.% loading of Pt in $Pt_{NP\text{-}S}/TiO_2$ catalysts (Table S1 in the ESM) also indicated the successful transfer of Pt into TiO_2 matrix. Figure 1(g) displays the HAADF-STEM image of pre-prepared $Pt_{NP\text{-}L}$ with size distribution of 36 ± 9 nm (Fig. 1(h)). According to the HAADF- STEM and TEM images of SPDR-made $Pt_{NP\text{-}L}/Al_2O_3$ (Fig. 1(i) and Fig. S5 in the ESM) and $Pt_{NP\text{-}L}/TiO_2$ (Fig. 1(j) and Fig. S6 in the ESM) catalysts, the $Pt_{NP\text{-}L}$ are also successfully transferred to Al_2O_3 and TiO_2 support, respectively. Due to the much larger size of $Pt_{NP\text{-}L}$ in $Pt_{NP\text{-}L}/Al_2O_3$ and $Pt_{NP\text{-}L}/TiO_2$, the particle densities are much lower than that of $Pt_{NP\text{-}S}$ in $Pt_{NP\text{-}S}/Al_2O_3$ and $Pt_{NP\text{-}S}/TiO_2$. The direct transfer of pre-prepared $Pt_{NP\text{-}S}$ and $Pt_{NP\text{-}L}$ nanoparticles from colloid into metal oxide matrix by SPDR not only endows a consistency in the preparation of catalysts, but also ensures the purity and uniformity of Pt species to obtain true signals of $Pt_{NP\text{-}S}$ and $Pt_{NP\text{-}L}$ in the following characterizations and catalysis. The Pt loading in the used catalysts was well controlled around 0.3 wt.% (Table S1 in the ESM).

The X-ray absorption near-edge structure (XANES) (Fig. 2(a)) and extended X-ray absorption fine spectra (EXAFS) (Figs. 2(b) and (c)) of Pt L_3-edge on synchrotron radiation were performed to study the chemical state of supported Pt species in Pt_1/TiO_2 (black curves), $Pt_{NP\text{-}S}/TiO_2$ (red curves), $Pt_{NP\text{-}L}/TiO_2$ (green curves), Pt_1/Al_2O_3 (orange curves), $Pt_{NP\text{-}S}/Al_2O_3$ (cyan curves), and $Pt_{NP\text{-}L}/Al_2O_3$ (magenta curves) with metallic Pt foil (blue curves) as reference. All the catalysts were calcined in air at 400 °C for two hours. According to XANES, the electron binding energies and intensities of white lines of Pt in both Pt_1/TiO_2 and Pt_1/Al_2O_3 catalysts are highest, indicating the highest oxidation state of Pt [4]. The oxidation states of Pt in both $Pt_{NP\text{-}L}/TiO_2$ and $Pt_{NP\text{-}L}/Al_2O_3$ are nearly to the metallic Pt, which is corresponded to the lowest intensities of white lines. However, the oxidation states of small $Pt_{NP\text{-}S}$ are depended on their supports: The Pt in $Pt_{NP\text{-}S}/TiO_2$ presents nearly full oxidation

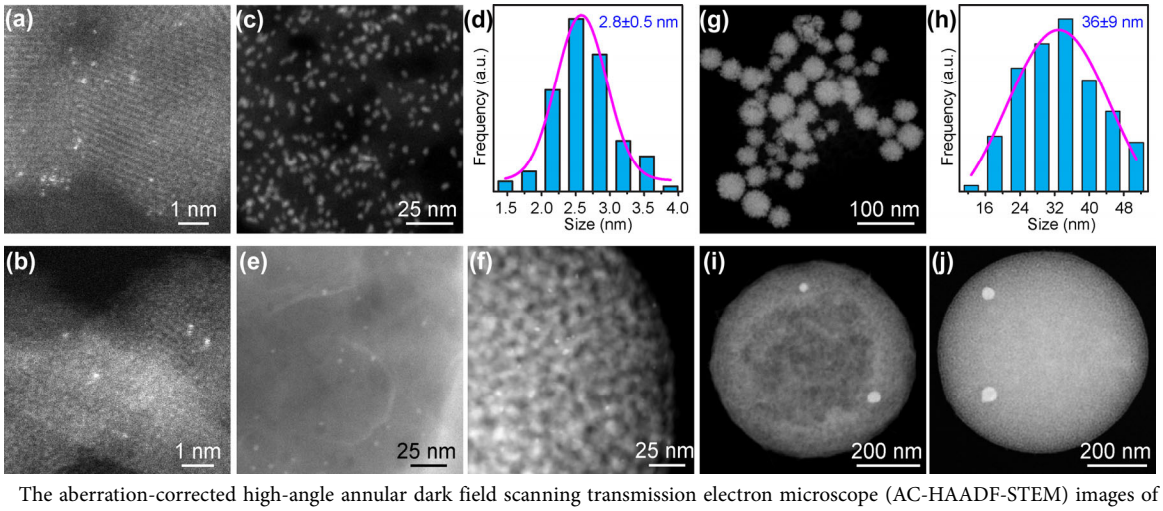

Figure 1 The aberration-corrected high-angle annular dark field scanning transmission electron microscope (AC-HAADF-STEM) images of Pt_1/TiO_2 (a) and Pt_1/Al_2O_3 (b) catalysts. The HAADF-STEM images ((c) and (g)) and size distribution ((d) and (h)) of $Pt_{NP\text{-}S}$ ((c) and (d)) and $Pt_{NP\text{-}L}$ ((g) and (h)), SPDR-made $Pt_{NP\text{-}S}/Al_2O_3$ (e), $Pt_{NP\text{-}S}/TiO_2$ (f), $Pt_{NP\text{-}L}/Al_2O_3$ (i), and $Pt_{NP\text{-}L}/TiO_2$ (j) catalysts.

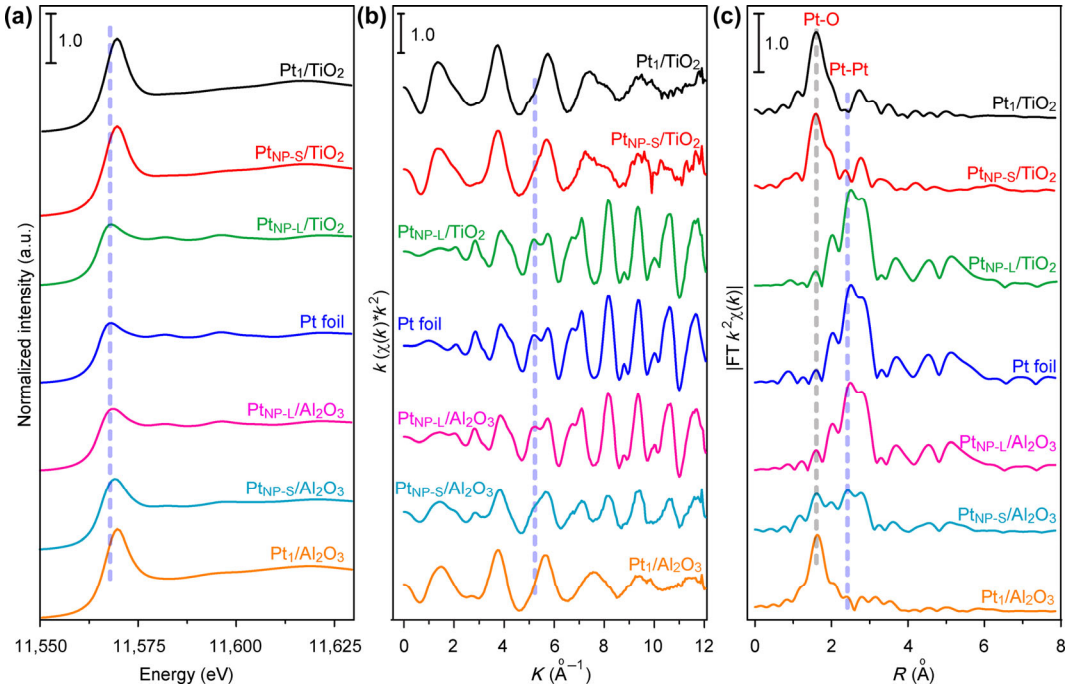

Figure 2 The X-ray absorption near-edge structure (XANES) (a) and extended X-ray absorption fine spectra (EXAFS) spectra in k^2-weighted Fourier transform (FT) *K*-space (b) and *R*-space (c) of Pt L_3-edge in Pt_1/TiO_2, $Pt_{NP\text{-}S}/TiO_2$, $Pt_{NP\text{-}L}/TiO_2$, Pt_1/Al_2O_3, $Pt_{NP\text{-}S}/Al_2O_3$, and $Pt_{NP\text{-}L}/Al_2O_3$ catalysts and metallic Pt foil.

state while the Pt in $Pt_{NP\text{-}S}/Al_2O_3$ shows an intermediate oxidation state between that in $Pt_{NP\text{-}L}/Al_2O_3$ and Pt_1/Al_2O_3. Besides, the binding energy peak of Pt in $Pt_{NP\text{-}S}/TiO_2$ shifted more than that in $Pt_{NP\text{-}S}/Al_2O_3$, further revealing their difference of oxidation state of Pt. The EXAFS study in k^2-weighted *K*-space (Fig. 2(b)) and *R*-space (Fig. 2(c)) of Pt L_3-edge further verifies the results from XANES. Vividly depicted in the R-spaced spectra, only Pt–O coordination was observed in Pt_1/TiO_2 and Pt_1/Al_2O_3 catalysts, which is consistent with AC-HAADF-STEM images and XANES. In both $Pt_{NP\text{-}L}/TiO_2$ and $Pt_{NP\text{-}L}/Al_2O_3$ catalysts, the Pt–Pt coordination was very close to that in Pt foil and Pt–O coordination was invisible, indicating the highly metallic state of larger $Pt_{NP\text{-}L}$. However, the coordination of smaller $Pt_{NP\text{-}S}$ in $Pt_{NP\text{-}S}/TiO_2$ and $Pt_{NP\text{-}S}/Al_2O_3$ was quite different. The metallic state Pt is notably decreased in comparison with the larger $Pt_{NP\text{-}L}$, indicating smaller Pt particles can be oxidized more easily. Moreover, the signal of metallic state Pt in $Pt_{NP\text{-}S}/TiO_2$ was notably weaker than that in $Pt_{NP\text{-}S}/Al_2O_3$, which suggests the much larger oxidation depth of $Pt_{NP\text{-}S}$ in $Pt_{NP\text{-}S}/TiO_2$, which stems from the well-known strong metal-support interactions (SMSI) [31, 54]. Therefore, the chemical property of supported Pt is highly depended on dual dispersion of Pt and property of support.

The model reaction of CO catalytic oxidation was performed to investigate the dual dispersion state and property of support induced activity of Pt/metal oxide catalysts in a fixed bed reactor. The feed gas was 1.0% CO + 1.0% O_2 + 98% He with a space velocity of 15,000 $mL \cdot h^{-1} \cdot g^{-1}$. Figure 3(a) presents the typical results of Pt_1/TiO_2 (red triangle plots), $Pt_{NP\text{-}S}/TiO_2$ (blue triangle plots), $Pt_{NP\text{-}L}/TiO_2$ (black triangle plots), Pt_1/Al_2O_3 (red square plots), $Pt_{NP\text{-}S}/Al_2O_3$ (red square plots), and $Pt_{NP\text{-}L}/Al_2O_3$ (red square plots). Herein, the contribution of supports was ignored because there is no any conversion of CO in both TiO_2 (magenta triangle, Fig. S7 in the ESM) and Al_2O_3 (magenta square, Fig. S8 in the ESM) supports at 300 °C. Firstly, it presents an obvious influence of dispersion on the performance in both Pt/TiO_2 and Pt_1/Al_2O_3. In Pt/TiO_2 system, it presents a performance order of Pt_1/TiO_2 >> $Pt_{NP\text{-}S}/TiO_2$ >> $Pt_{NP\text{-}L}/TiO_2$. While in Pt/Al_2O_3 system, it presents an interesting order of $Pt_{NP\text{-}S}/Al_2O_3$ > Pt_1/Al_2O_3 >> $Pt_{NP\text{-}L}/Al_2O_3$. The performance of larger $Pt_{NP\text{-}L}$ is the worst no matter which support they are loaded on. However, the performance of Pt_1 is quite different, indicating a strong effect of support, which will be discussed subsequently. The apparent activation energies (E_{app}, Fig. 3(b)) based on Arrhenius fitting further confirmed the dispersion-depended activity. In Pt/TiO_2 system, the E_{app} values of Pt_1/TiO_2, $Pt_{NP\text{-}S}/TiO_2$, and $Pt_{NP\text{-}L}/TiO_2$ are 55.9, 57.0 and 81.0 kJ/mol.

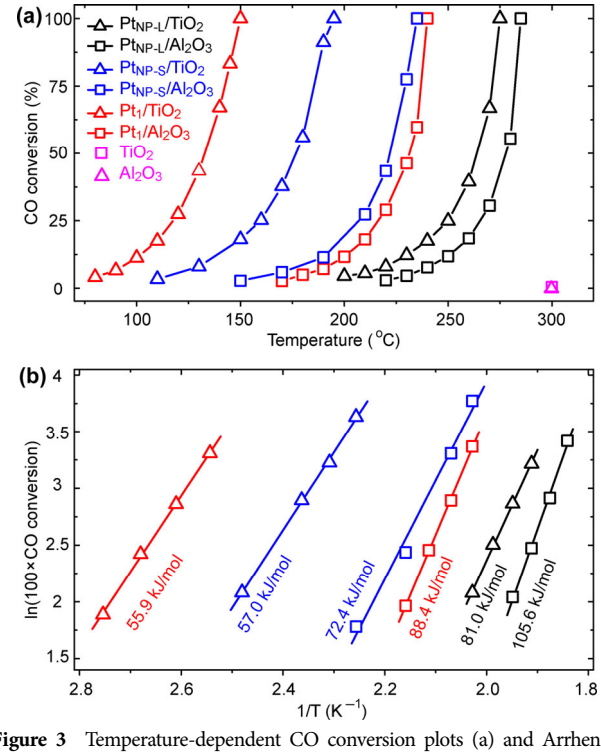

Figure 3 Temperature-dependent CO conversion plots (a) and Arrhenius fitting plots (b) of Pt_1/TiO_2, $Pt_{NP\text{-}S}/TiO_2$, $Pt_{NP\text{-}L}/TiO_2$, Pt_1/Al_2O_3, $Pt_{NP\text{-}S}/Al_2O_3$, and $Pt_{NP\text{-}L}/Al_2O_3$ catalysts and pristine TiO_2 and Al_2O_3 supports.

Almost the same E_{app} values but contrasting CO oxidation efficiency indicate (1) the activity of both Pt_1/TiO_2 and Pt_{NP-S}/TiO_2 stems from the Pt–O–Ti sites [43, 44, 55]; (2) the single-atom dispersion endows Pt_1/TiO_2 much more Pt–O–Ti sites than Pt_{NP-S}/TiO_2 and therefore brings 45 °C lower temperature for 100% conversion of CO (T_{100}). The much higher E_{app} value in Pt_{NP-L}/TiO_2 suggests increasing size of Pt particles not only loses the surface exposed Pt atoms but also makes the active Pt–O–Ti sites less and less contribution to the CO oxidation. Revisiting the EXAFS results, we can understand the catalytic behaviors of TiO_2 supported Pt species. For Pt_{NP-S}/TiO_2, although the reducible TiO_2 brings a SMSI effect and nearly full oxidation state of Pt, the lower dispersity leads to a much lower catalytic performance. For Pt_{NP-L}/TiO_2, the disappearance of oxidized Pt indicates the ratio of interfacial Pt–O–Ti sites is quite low. When the size of Pt is larger than the interfacial depth of Pt/TiO_2, the effect of TiO_2 is negligible on surface property of Pt_{NP-L} nanoparticles. As a result, the surface and catalytic property of Pt_{NP-L} was quite different from that of TiO_2 supported both Pt_1 and Pt_{NP-S}. Limited by both low dispersion and inferior Pt state, the T_{100} difference reaches 125 °C between Pt_{NP-L}/TiO_2 and Pt_1/TiO_2 in CO oxidation.

The results in both Pt/TiO_2 and Pt/Al_2O_3 system reveal the dispersion regulated activity of Pt species. Nevertheless, the influence of support on the activity was also very dominant due to the influence of dispersion was quite different between Pt/TiO_2 and Al_2O_3 system. More interestingly, the T_{100} in Pt_1/TiO_2 (150 °C) was 90 °C lower than that in Pt_1/Al_2O_3 (240 °C) although both of them possess single-atom dispersion of Pt. Meanwhile, the T_{100} differences between Pt_{NP-S}/TiO_2 (195 °C) and Pt_{NP-S}/Al_2O_3 (235 °C), Pt_{NP-L}/TiO_2 (275 °C) and Pt_{NP-L}/Al_2O_3 (285 °C) were 40 °C and 10 °C, respectively. All the Pt species supported on reducible TiO_2 present superior performance than the corresponding ones supported on "inert" Al_2O_3. The E_{app} values further confirmed the support-depended activity. All the E_{app} values in Pt_1/Al_2O_3, Pt_{NP-S}/Al_2O_3, and Pt_{NP-L}/Al_2O_3 are higher than the corresponding Pt_1/TiO_2, Pt_{NP-S}/TiO_2, and Pt_{NP-L}/TiO_2 catalysts. Furthermore, the influence of support on the performance is decreased with the rising of size of Pt. The T_{100} difference between Pt_1/Al_2O_3 and Pt_1/TiO_2 reaches 90 °C while it narrows to just 10 °C between Pt_{NP-L}/TiO_2 and Pt_{NP-L}/Al_2O_3. As discussed in EXAFS results that Pt in both Pt_{NP-L}/TiO_2 and Pt_{NP-L}/Al_2O_3 presents metallic state, we think that activity is mainly determined by the supported Pt_{NP-L} particles when the size of Pt is larger than the interfacial depth of Pt/TiO_2 or Pt/Al_2O_3.

Above all, a reducible metal oxide is critical to endow Pt–O–M (metal) site a high activity and single-atom dispersion of Pt is the way to maximize Pt–O–M sites. In other words, the efficiency is affected by the dispersion of Pt while the activity is determined by the property of support. To explore the origin of the influence of reducible TiO_2 support on the activity, a density function theory (DFT) study (Fig. 4) was performed to investigate the reaction pathway of CO oxidation at Pt–O–Ti sites with the model surfaces of sing-atom Pt_1/TiO_2 catalysts. According to the X-ray diffraction (XRD) pattern (Fig. S1(d) in the ESM) of Pt_1/TiO_2 and Thang et al.'s work [56, 57], we propose the single Pt atoms were stably adsorbed on anatase TiO_2 (101) terraces and bridge-type bonded with two O atoms (configuration IV). The CO oxidation cycles on Pt_1/TiO_2 consisted of five steps, associated with five intermediate configurations I to V and two chemical reactions. The dissociation adsorption of O_2 molecule led to a lattice O to fill surface oxygen vacancy (O_v) of configuration I and form an adsorbed O. The Reaction-I with step of III-IV met Langmuir–Hinshelwood (L–H) mechanism [4, 58, 59] with a barrier (E_{a1}) of 27.8 kJ/mol, where the adsorbed O moved to the adjacent CO activated on Pt_1 sites to form a CO_2 molecule. However, the Reaction-II with step of V-I satisfied the Mars-van Krevelen (M–K) mechanism [60, 61], where the lattice O participated in the Reaction-II to release the other CO_2 molecule. The transition state searching (TS-2) suggested that the Reaction-II is the rate determining step with E_{a2} of 44.2 kJ/mol, close to the experimental result (55.9 kJ/mol). The low E_{a2} well met the knowledge that the supported metal species can efficiently promote lattice oxygen removal from oxide surfaces [62]. In Reaction-II, the lattice O atom at Pt_1–O–Ti site was consumed by the adjacent CO adsorbed on Pt, producing a CO_2 molecule and leaving a surface O_v. Thus, the energy of O_v formation (E_{Ov}) significantly affected the value of E_{a2}. Besides, the surface metal–oxygen (M–O) bond at Pt_1–O–M site is broken with the formation of O_v, so the reducibility diversity of metal oxide support was response to the E_{Ov} differences of Pt_1–O–M site. As shown in Fig. S9 in the ESM, the E_{Ov} on Pt_1/Al_2O_3 (304.3 kJ/mol) was notably higher than that on Pt_1/TiO_2 (214.1 kJ/mol). Resultantly, the CO oxidation reaction on Pt_1/Al_2O_3 were found to follow non-oxygen vacancy pathway [28, 63]. In Gao' work [63], a O*–O–C = O_2* intermediate pathway for Pt_1/Al_2O_3 was confirmed and the reaction barrier in rate determination step was 80.7 kJ/mol, which was highly consistent with our experimental result (88.4 kJ/mol). Therefore, the surface E_{Ov} value is chemical source for regulating the reaction pathway and activity of metal oxide supports.

The DFT study was also conducted on the catalytic property of Pt–O–Ti with single atom Pt substitutional to surface lattice Ti (Pt_1/TiO_2–S). Figure S10 in the ESM presented an E_{a2} value of

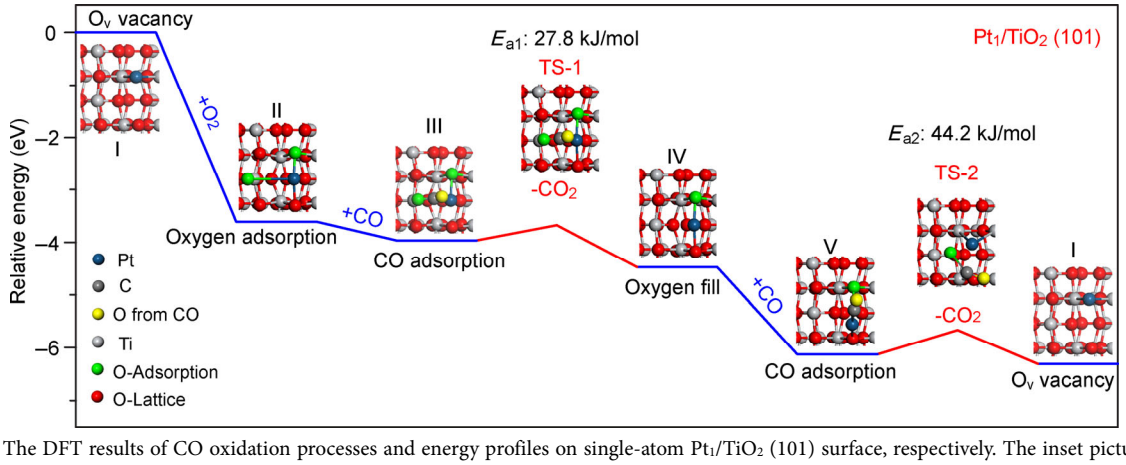

Figure 4 The DFT results of CO oxidation processes and energy profiles on single-atom Pt_1/TiO_2 (101) surface, respectively. The inset pictures are the stable configurations of catalysts' surface at various reactions steps, and the TS-1 and TS-2 are the two translation state configurations.

52.8 kJ/mol, which was close to the values discussed above with Pt adsorbed on surface with coordination to surface oxygen. It suggests that the E_{Ov} plays more important role in determining the barrier of CO oxidation than the surface structure of Pt_1–O–Ti sites. To confirm the support regulated activity of Pt, other SPDR-made Pt/metal oxide catalysts, such as Pt/CeO_2, Pt/Co_3O_4, Pt/CuO, Pt_1/NiO, and Pt_1/ZnO were further investigated. As shown in Fig. S11 in the ESM, it appears different performance at low-temperate region, which is indexed to the difference of redox properties of supports. Besides, we find an excellent catalyst Pt/Co_3O_4, which exhibits the best performance among the investigated samples.

4 Conclusions

In summary, this work clarifies dispersion and support dictated activities of Pt by investigating single-atom (Pt_1), 2.8 nm ($Pt_{NP\text{-}S}$) and 36 nm ($Pt_{NP\text{-}L}$) Pt supported on both reducible (e.g., TiO_2) and "inert" (e.g., Al_2O_3) metal oxides. The chemical state of supported Pt species is affected by both dispersion state and property of support. The dual dispersion and support dictated chemical state of Pt is found to determine the activity of Pt/metal oxide catalysts. A reducible metal oxide is critical to endow Pt–O–M (metal) site a high activity and the single-atom dispersion of Pt is the way to maximize Pt–O–M sites. Therefore, this work clearly elucidates a fundamental understanding on the origin of activity of Pt on metal oxides with size ranging from single-atom to dozens of nanometers, and provides a comprehensive guidance for the activity control of supported Pt catalysts.

Acknowledgements

This work was financially supported by the National Natural Science Foundation of China (Nos. 21801003 and 21871005), the Natural Science Foundation of Anhui Province (No. 1808085QB47), the University Synergy Innovation Program of Anhui Province (No. GXXT-2020-005), Fund for Outstanding Youth of Anhui Polytechnic University (Nos. 2019JQ01 and 2016BJRC001). The authors thank the National Synchrotron Radiation Laboratory (Beijing) for EXAFS collection and Hangzhou Precision New Materials and Technology Co., Ltd. (Hangzhou, China) for the DFT study.

Electronic Supplementary Material: Supplementary material (additional experimental details, additional figures, tables, notes and references) is available in the online version of this article at https://doi.org/10.1007/s12274-021-3443-7.

References

[1] Lin, J.; Wang, X. D.; Zhang, T. Recent progress in CO oxidation over Pt-group-metal catalysts at low temperatures. *Chin. J. Catal.* **2016**, *37*, 1805–1813.

[2] Jones, J.; Xiong, H. F.; DeLaRiva, A. T.; Peterson, E. J.; Pham, H.; Challa, S. R.; Qi, G.; Oh, S.; Wiebenga, M. H.; Hernández, X. I. P. et al. Thermally stable single-atom platinum-on-ceria catalysts via atom trapping. *Science* **2016**, *353*, 150–154.

[3] Qiao, B. T.; Wang, A. Q.; Yang, X. F.; Allard, L. F.; Jiang, Z.; Cui, Y. T.; Liu, J. Y.; Li, J.; Zhang, T. Single-atom catalysis of CO oxidation using Pt_1/FeO_x. *Nat. Chem.* **2011**, *3*, 634–641.

[4] Cao, L. N.; Liu, W.; Luo, Q. Q.; Yin, R. T.; Wang, B.; Weissenrieder, J.; Soldemo, M.; Yan, H.; Lin, Y.; Sun, Z. H. et al. Atomically dispersed iron hydroxide anchored on Pt for preferential oxidation of CO in H_2. *Nature* **2019**, *565*, 631–635.

[5] Zhang, L. L.; Zhou, M. X.; Wang, A. Q.; Zhang, T. Selective hydrogenation over supported metal catalysts: From nanoparticles to single atoms. *Chem. Rev.* 2020, *120*, 683–733.

[6] Wen, J. F.; Chen, Y. J.; Ji, S. F.; Zhang, J.; Wang, D. S.; Li, Y. D. Metal-organic frameworks-derived nitrogen-doped carbon supported nanostructured PtNi catalyst for enhanced hydrosilylation of 1-octene. *Nano Res.* **2019**, *12*, 2584–2588.

[7] Chen, G. X.; Xu, C. F.; Huang, X. Q.; Ye, J. Y.; Gu, L.; Li, G.; Tang, Z. C.; Wu, B. H.; Yang, H. Y.; Zhao, Z. P. et al. Interfacial electronic effects control the reaction selectivity of platinum catalysts. *Nat. Mater.* 2016, *15*, 564–569.

[8] Fu, Q.; Saltsburg, H.; Flytzani-Stephanopoulos, M. Active nonmetallic Au and Pt species on ceria-based water-gas shift catalysts. *Science* 2003, *301*, 935–938.

[9] Zhai, Y. P.; Pierre, D.; Si, R.; Deng, W. L.; Ferrin, P.; Nilekar, A. U.; Peng, G. W.; Herron, J. A.; Bell, D. C.; Saltsburg, H. et al. Alkali-stabilized Pt-OH_x species catalyze low-temperature water-gas shift reactions. *Science* 2010, *329*, 1633–1636.

[10] de Lima, S. M.; da Cruz, I. O.; Jacobs, G.; Davis, B. H.; Mattos, L. V.; Noronha, F. B. Steam reforming, partial oxidation, and oxidative steam reforming of ethanol over Pt/$CeZrO_2$ catalyst. *J. Catal.* 2008, *257*, 356–368.

[11] Lin, L. L.; Zhou, W.; Cao, R.; Yao, S. Y.; Zhang, X.; Xu, W. Q.; Zheng, S. J.; Jiang, Z.; Yu, Q. L.; Li, Y. W. et al. Low-temperature hydrogen production from water and methanol using Pt/α-MoC catalysts. *Nature* **2017**, *544*, 80–83.

[12] Zhang, N. Q.; Ye, C. L.; Yan, H.; Li, L. C.; He, H.; Wang, D. S.; Li, Y. D. Single-atom site catalysts for environmental catalysis. *Nano Res.* **2020**, *13*, 3165–3182.

[13] Lang, R.; Du, X. R.; Huang, Y. K.; Jiang, X. Z.; Zhang, Q.; Guo, Y. L.; Liu, K. P.; Qiao, B. T.; Wang, A. Q.; Zhang, T. Single-atom catalysts based on the metal-oxide interaction. *Chem. Rev.* **2020**, *120*, 11986–12043.

[14] Wang, A. Q.; Li, J.; Zhang, T. Heterogeneous single-atom catalysis. *Nat. Rev. Chem.* **2018**, *2*, 65–81.

[15] Chen, Z.; Yang, W. J.; Wu, Y.; Zhang, C.; Luo, J.; Chen, C.; Li, Y. D. Atomic iron on mesoporous N-doped carbon to achieve dehydrogenation reaction at room temperature. *Nano Res.* **2020**, *13*, 3075–3081.

[16] Cao, S. F.; Yang, M.; Elnabawy, A. O.; Trimpalis, A.; Li, S.; Wang, C. Y.; Göltl, F.; Chen, Z. H. Y.; Liu, J. L.; Shan, J. J. et al. Single-atom gold oxo-clusters prepared in alkaline solutions catalyse the heterogeneous methanol self-coupling reactions. *Nat. Chem.* **2019**, *11*, 1098–1105.

[17] Yang, M.; Li, S.; Wang, Y.; Herron, J. A.; Xu, Y.; Allard, L. F.; Lee, S.; Huang, J.; Mavrikakis, M.; Flytzani-Stephanopoulos, M. Catalytically active Au-$O(OH)_x^-$ species stabilized by alkali ions on zeolites and mesoporous oxides. *Science* **2014**, *346*, 1498–1501.

[18] Gates, B. C.; Flytzani-Stephanopoulos, M.; Dixon, D. A.; Katz, A. Atomically dispersed supported metal catalysts: Perspectives and suggestions for future research. *Catal. Sci. Technol.* **2017**, *7*, 4259–4275.

[19] Wu, K. L.; Chen, X.; Liu, S. J.; Pan, Y.; Cheong, W. C.; Zhu, W.; Cao, X.; Shen, R. A.; Chen, W. X.; Luo, J. et al. Porphyrin-like Fe-N_4 sites with sulfur adjustment on hierarchical porous carbon for different rate-determining steps in oxygen reduction reaction. *Nano Res.* **2018**, *11*, 6260–6269.

[20] Sun, T. T.; Xu, L. B.; Wang, D. S.; Li, Y. D. Metal organic frameworks derived single atom catalysts for electrocatalytic energy conversion. *Nano Res.* **2019**, *12*, 2067–2080.

[21] Pan, Y.; Zhang, C.; Lin, Y.; Liu, Z.; Wang, M. M.; Chen, C. Electrocatalyst engineering and structure-activity relationship in hydrogen evolution reaction: From nanostructures to single atoms. *Sci. China Mater.* **2020**, *63*, 921–948.

[22] Ding, K. L.; Gulec, A.; Johnson, A. M.; Schweitzer, N. M.; Stucky, G. D.; Marks, L. D.; Stair, P. C. Identification of active sites in CO oxidation and water-gas shift over supported Pt catalysts. *Science* **2015**, *350*, 189–192.

[23] Maurer, F.; Jelic, J.; Wang, J. J.; Gänzler, A.; Dolcet, P.; Wöll, C.; Wang, Y. M.; Studt, F.; Casapu, M.; Grunwaldt, J. D. Tracking the formation, fate and consequence for catalytic activity of Pt single sites on CeO_2. *Nat. Catal.* **2020**, *3*, 824–833.

[24] Therrien, A. J.; Hensley, A. J. R.; Marcinkowski, M. D.; Zhang, R. Q.; Lucci, F. R.; Coughlin, B.; Schilling, A. C.; McEwen, J. S.;

Sykes, E. C. H. An atomic-scale view of single-site Pt catalysis for low-temperature CO oxidation. *Nat. Catal.* **2018**, *1*, 192–198.
[25] Nie, L.; Mei, D. H.; Xiong, H. F.; Peng, B.; Ren, Z. B.; Hernandez, X. I. P.; DeLaRiva, A.; Wang, M.; Engelhard, M. H.; Kovarik, L. et al. Activation of surface lattice oxygen in single-atom Pt/CeO_2 for low-temperature CO oxidation. *Science* **2017**, *358*, 1419–1423.
[26] Chen, W. L.; Ma, Y. L.; Li, F.; Pan, L.; Gao, W. P.; Xiang, Q.; Shang, W.; Song, C. Y.; Tao, P.; Zhu, H. et al. Strong electronic interaction of amorphous Fe_2O_3 nanosheets with single-atom Pt toward enhanced carbon monoxide oxidation. *Adv. Funct. Mater.* **2019**, *29*, 1904278.
[27] Zhang, Z. L.; Zhu, Y. H.; Asakura, H.; Zhang, B.; Zhang, J. G.; Zhou, M. X.; Han, Y.; Tanaka, T.; Wang, A. Q.; Zhang, T. et al. Thermally stable single atom Pt/m-Al_2O_3 for selective hydrogenation and CO oxidation. *Nat. Commun.* **2017**, *8*, 16100.
[28] Moses-DeBusk, M.; Yoon, M.; Allard, L. F.; Mullins, D. R.; Wu, Z. L.; Yang, X. F.; Veith, G.; Stocks, G. M.; Narula, C. K. CO oxidation on supported single Pt atoms: Experimental and ab initio density functional studies of CO interaction with Pt atom on θ-Al_2O_3(010) surface. *J. Am. Chem. Soc.* **2013**, *135*, 12634–12645.
[29] Wang, H.; Liu, J. X.; Allard, L. F.; Lee, S.; Liu, J. L.; Li, H.; Wang, J. Q.; Wang, J.; Oh, S. H.; Li, W. et al. Surpassing the single-atom catalytic activity limit through paired Pt-O-Pt ensemble built from isolated Pt_1 atoms. *Nat. Commun.* **2019**, *10*, 3808.
[30] Beniya, A.; Higashi, S.; Ohba, N.; Jinnouchi, R.; Hirata, H.; Watanabe, Y. CO oxidation activity of non-reducible oxide-supported mass-selected few-atom Pt single-clusters. *Nat. Commun.* **2020**, *11*, 1888.
[31] van Deelen, T. W.; Mejía, C. H.; de Jong, K. P. Control of metal-support interactions in heterogeneous catalysts to enhance activity and selectivity. *Nat. Catal.* **2019**, *2*, 955–970.
[32] Jiao, J. Q.; Pan, Y.; Wang, B.; Yang, W. J.; Liu, S. J.; Zhang, C. Melamine-assisted pyrolytic synthesis of bifunctional cobalt-based core-shell electrocatalysts for rechargeable zinc–air batteries. *J. Energy Chem.* **2021**, *53*, 364–371.
[33] Liu, K. P.; Zhao, X. T.; Ren, G. Q.; Yang, T.; Ren. Y. J.; Lee, A. F.; Su, Y.; Pan, X. L.; Zhang, J. C.; Chen, Z. Q. et al. Strong metal-support interaction promoted scalable production of thermally stable single-atom catalysts. *Nat. Commun.* **2020**, *11*, 1263.
[34] Tang, Y.; Wang, Y. G.; Li, J. Theoretical investigations of Pt_1@CeO_2 single-atom catalyst for CO oxidation. *J. Phys. Chem. C* **2017**, *121*, 11281–11289.
[35] Wang, C. L.; Gu X. K.; Yan, H.; Lin, Y.; Li, J. J.; Liu, D. D.; Li, W. X.; Lu, J. L. Water-mediated Mars-Van Krevelen mechanism for CO Oxidation on ceria-supported single-atom Pt_1 catalyst. *ACS Catal.* **2017**, *7*, 887–891.
[36] Wang, J.; Huang, Z. Q.; Liu, W.; Chang, C. R.; Tang, H. L.; Li, Z. J.; Chen, W. X.; Jia, C. J.; Yao, T.; Wei, S. Q. et al. Design of N-coordinated dual-metal sites: A stable and active Pt-free catalyst for acidic oxygen reduction reaction. *J. Am. Chem. Soc.* **2017**, *139*, 17281–17284.
[37] Zhao, Y. Y.; Yang, K. R.; Wang, Z. C.; Yan, X. X.; Cao, S. F.; Ye, Y. F.; Dong, Q.; Zhang, X. Z.; Thorne, J. E.; Jin, L. et al. Stable iridium dinuclear heterogeneous catalysts supported on metal-oxide substrate for solar water oxidation. *Proc. Natl. Acad. Sci. USA* **2018**, *115*, 2902–2907.
[38] Qin, R. X.; Liu, K. L.; Wu, Q. Y.; Zheng, N. F. Surface coordination chemistry of atomically dispersed metal catalysts. *Chem. Rev.* **2020**, *120*, 11810–11899.
[39] Li, H. N.; Cao, C. Y.; Liu, J.; Shi, Y.; Si, R.; Gu, L.; Song, W. G. Cobalt single atoms anchored on N-doped ultrathin carbon nanosheets for selective transfer hydrogenation of nitroarenes. *Sci. China Mater.* **2019**, *62*, 1306–1314.
[40] Kuai, L.; Chen, Z.; Liu, S. J.; Kan, E. J.; Yu, N.; Ren, Y. M.; Fang, C. H.; Li, X. Y.; Li, Y. D.; Geng, B. Y. Titania supported synergistic palladium single atoms and nanoparticles for room temperature ketone and aldehydes hydrogenation. *Nat. Commun.* **2020**, *11*, 48.
[41] Wei, H. S.; Liu, X. Y.; Wang, A. Q.; Zhang, L. L.; Qiao, B. T.; Yang, X. F.; Huang, Y. Q.; Miao, S.; Liu, J. Y.; Zhang, T. FeO_x-supported platinum single-atom and pseudo-single-atom catalysts for chemoselective hydrogenation of functionalized nitroarenes. *Nat. Commun.* **2014**, *5*, 5634.
[42] Kwak, J. H.; Kovarik, L.; Szanyi, J. Heterogeneous catalysis on atomically dispersed supported metals: CO_2 reduction on multifunctional Pd catalysts. *ACS Catal.* **2013**, *3*, 2094–2100.
[43] Allard, L. F.; Borisevich, A.; Deng, W. L.; Si, R.; Flytzani-Stephanopoulos, M.; Overbury, S. H. Evolution of gold structure during thermal treatment of Au/FeO_x catalysts revealed by aberration-corrected electron microscopy. *J. Electron Microsc.* **2009**, *58*, 199–212.
[44] Kuai, L.; Liu, S. J.; Cao, S. F.; Ren, Y. M.; Kan, E. J.; Zhao, Y. Y.; Yu, N.; Li, F.; Li, X. Y.; Wu, Z. C. et al. Atomically dispersed Pt/metal oxide mesoporous catalysts from synchronous pyrolysis-deposition route for water-gas shift reaction. *Chem. Mater.* **2018**, *30*, 5534–5538.
[45] Xiang, Y. P.; He, J.; Sun, N.; Fan, Y. T; Yang, L. M.; Fang, C. H.; Kuai, L. Hollow mesoporous CeO_2 microspheres for efficient loading of Au single-atoms to catalyze the water-gas shift reaction. *Microp. Mesop. Mater.* **2020**, *308*, 110507.
[46] Kan, E. J.; Kuai, L.; Wang, W. H.; Geng, B. Y. Delivery of highly active noble-metal nanoparticles into microspherical supports by an aerosol-spray method. *Chem. Eur. J.* **2015**, *21*, 13291–13296.
[47] Teranishi, T.; Hosoe, M.; Tanaka, T.; Miyake, M. Size control of monodispersed Pt nanoparticles and their 2D organization by electrophoretic deposition. *J. Phys. Chem. B* **1999**, *103*, 3818–3827.
[48] Wang, S. Z.; Kuai, L.; Huang, Y. C.; Yu, X.; Liu, Y. D.; Li, W. Z.; Chen, L.; Geng, B. Y. A highly efficient, clean-surface, porous platinum electrocatalyst and the inhibition effect of surfactants on catalytic activity. *Chem. Eur. J.* **2013**, *19*, 240–248.
[49] Segall, M. D.; Lindan, P. J. D.; Probert, M. J.; Pickard, C. J.; Hasnip, P. J.; Clark S. J.; Payne, M. C. First-principles simulation: Ideas, illustrations and the CASTEP code. *J. Phys.: Condens. Matter* **2002**, *14*, 2717.
[50] Perdew, J. P.; Burke, K.; Ernzerhof, M. Generalized gradient approximation made simple. *Phys. Rev. Lett.* **1996**, *77*, 3865.
[51] Hamann, D. R.; Schlüter, M.; Chiang, C. Norm-conserving pseudopotentials. *Phys. Rev. Lett.* **1979**, *43*, 1494–1497.
[52] Li, C.; Zhao, Y. F.; Gong, Y. Y.; Wang, T.; Sun, C. Q. Band gap engineering of early transition-metal-doped anatase TiO_2: First principles calculations. *Phys. Chem. Chem. Phys.* **2014**, *16*, 21446–21451.
[53] Yan, D. X.; Liu, Q.; Zeng, C.; Dong, N. B.; Huang, Y. D.; Xiao, W. Adsorption of lithium polysulfides on an anatase (101) and an α-Al_2O_3(0001) surface under external electric field with first principles calculations. *Appl. Surf. Sci.* **2019**, *463*, 331–338.
[54] Xu, B.; Yang, H.; Zhou, G.; Wang, X. Strong metal-support interaction in size-controlled monodisperse palladium-hematite nano-heterostructures during a liquid-solid heterogeneous catalysis. *Sci. China Mater.* **2014**, *57*, 34–41.
[55] Yang, M.; Liu, J. L.; Lee, S.; Zugic, B.; Huang, J.; Allard, L. F.; Flytzani-Stephanopoulos, M. A common single-site Pt(II)-$O(OH)_x$-species stabilized by sodium on "active" and "inert" supports catalyzes the water-gas shift reaction. *J. Am. Chem. Soc.* **2015**, *137*, 3470–3473.
[56] Thang, H. V.; Pacchioni, G.; Derita, L.; Christopher, P. Nature of stable single atom Pt catalysts dispersed on anatase TiO_2. *J. Catal.* **2018**, *367*, 104–114.
[57] DeRita, L.; Resasco, J.; Dai, S.; Boubnov, A.; Thang, H. V.; Hoffman, A. S.; Ro, I.; Graham, G. W.; Bare, S. R.; Pacchioni, G. et al. Structural evolution of atomically dispersed Pt catalysts dictates reactivity. *Nat. Mater.* **2019**, *18*, 746–751.
[58] Baxter, R. J.; Hu, P. Insight into why the Langmuir-Hinshelwood mechanism is generally preferred. *J. Chem. Phys.* **2002**, *116*, 4379.
[59] Ertl, G. Reactions at surfaces: From atoms to complexity (Nobel Lecture). *Angew. Chem., Int. Ed.* **2008**, *47*, 3524–3535.
[60] Qin, L.; Cui Y. Q.; Deng T. L.; Wei, F. H.; Zhang, X. F. Highly stable and active Cu_1/CeO_2 single-atom catalyst for CO oxidation: A DFT study. *ChemPhyChem* **2018**, *19*, 3346–3349.
[61] Thang, H. V.; Pacchioni, G. CO oxidation promoted by a Pt_4/TiO_2 catalyst: Role of lattice oxygen at the metal/oxide interface. *Catal. Lett.* **2019**, *149*, 390–398.
[62] Sanchez, M. G.; Gazquez, J. L. Oxygen vacancy model in strong metal-support interaction. *J. Catal.* **1987**, *104*, 120–135.
[63] Gao, H. W. CO oxidation mechanism on the γ-Al_2O_3 supported single Pt atom: First principle study. *Appl. Surf. Sci.* **2016**, *379*, 347–357.